Muscle-to-Motion: dual channel bio-signal acquisition, digitization, and robotics control

Magnus Støren Wedèn, Jon Martin Kvanum Hestnes, Dhanial Ditta, Maz Safdar
Oslo Metropolitan University

***Abstract*—This paper presents the design and implementation of a bio-signal-driven robotic control system based on electromyography (EMG) and photoplethysmography (PPG). Surface electrodes and optical sensors acquire muscle activation and cardiovascular pulse signals, which undergo amplification, filtering, and envelope extraction. The processed signals are digitized using a microcontroller and mapped to actuator commands that control a Braccio robotic arm. The developed system demonstrates a proof-of-concept of an intuitive human–machine interface with potential applications in rehabilitation, assistive robotics, and human–computer interaction.**

***Index Terms*—Electromyography; photoplethysmography; bio-signal processing; instrumentation amplifier; robotic control; biomedical sensors; signal conditioning**

I. Introduction

Electromyography (EMG) and photoplethysmography (PPG) offer complementary approaches to bio-signal acquisition. EMG evaluates and records electrical signals generated by active muscle fibers. For surface EMG, signal amplitudes typically lie in the upper microvolt range to several millivolts [1], with most of the spectral content concentrated between 10 and 500 Hz[2].

PPG, conversely, employs an optical method to track blood volume changes in tissue. This yields cardiovascular information in the frequency range of $\approx 0-5Hz$, providing a pulsatile signal suitable for heart-rate estimation.[3].

In combination, these technologies are applied to a variety of applications, including rehabilitation and training, robotic assistive devices, and prosthetics[4], [5], [6].

The signal processing architecture presented in Fig. 1 provides a simplified block representation of the signal flow and processing for both methods: from biological signal acquisition, through analog signal conditioning and digitization, to motor control.

Each sensor type requires independent, tailored analog signal paths. EMG signals demand a high-impedance instrumentation amplifier front end, whereas the PPG signal necessitates a trans-impedance amplifier to convert photo-diode current to voltage. Both circuits use similar noise-reduction strategies, relying on analog filtering to limit bandwidth and prevent unwanted noise amplification. Noise sources are numerous—crosstalk from adjacent muscles, electromagnetic pickup from wiring or ambient light, and mains interference—making adequate filtering essential.

To obtain *control voltages* suitable for robotic control from the EMG-signal, additional stages perform rectification and envelope shaping. An optical isolation stage provides galvanic isolation, while *protection* resistors limit accidental fault currents through the electrode interface and, consequently, the patient.

This paper details the theoretical foundations, circuit design considerations, and implementation challenges of the two bio-signal acquisition and processing chains, with emphasis on achieving suitable signal amplitudes and bandwidths for reliable digitization and robotic control.

II. Electromyography Sensor System

A. EMG electrode placement and considerations

Care must be taken in placing the electrodes, as poor placement increases the risk of crosstalk from adjacent muscles and can compromise the accuracy of the EMG measurement[1]. In our setup, the two differential electrodes were placed over the belly of the *biceps brachii*, approximately aligned with the center along the fiber direction. Skin preparation (abrasion) is recommended to minimize skin impedance [1], but was not performed in our experiment. The reference electrode was attached to a ”bony” area near the elbow. This reference electrode is tied to the REF pin of the INA and forms the primary side system ground. This, along with careful reference electrode placement, provides a stable common reference potential.

B. System overview

The scope of this project steers our efforts towards achieving suitable signal amplification and processing for motor control, as opposed to the narrow specifications required by a true medical device. Consequently, preserving full EMG-signal fidelity is of lesser importance than implementing the processing required to obtain reliable robotic actuation. Some safety requirements similar to those of a certified medical device, however, will be implemented. We are working with electrodes connected to the body on one side and an electric circuit on the other, so the potential for electric shock is present, and precautions are thus taken.

The analog sEMG system contains the following elements:

- (3) passive, 3M ”Red dot” one-use electrodes with detachable leads
- instrumentation preamplifier
- signal processing:
  - Filtering (noise reduction):
    - High-pass (low cut) filtering
    - Low-pass (high cut) filtering

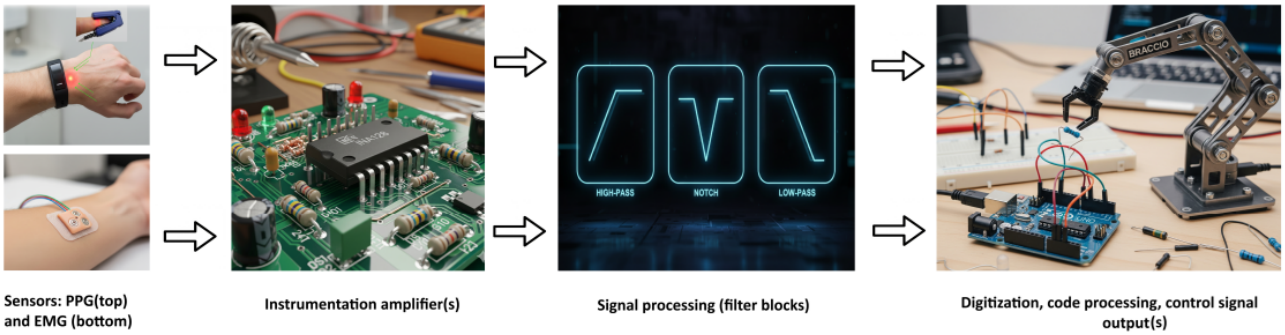

Fig. 1: Complete signal processing chain: EMG and PPG signals are amplified, bandwidth-shaped using highpass (20Hz for EMG, 0.5Hz for PPG), lowpass (500Hz for EMG, 5Hz for PPG), and 50 Hz notch filters, digitized via the Arduino ADC, and processed to produce control commands for the Braccio robotic arm. **Note**: there is some additional signal processing happening in the EMG-signal path within the "Signal processing" block which is detailed later in the report.

    - Notch (band-reject) filtering
  - Rectification and integration
- Circuit isolation
- Various gain-stages, dc-removal, and polarity-correcting amplifiers are utilized throughout as needed

C. Instrumentation Amplifier

TI INA128 was utilized as the system's main instrumentation preamplifier in the hardware implementation, while its equivalent dual version was used in the simulation. Different gain configurations were tested, and a $1\,\text{k}\Omega$ gain-setting resistor was chosen, giving: $A_v = 1 + \frac{50\,000\,\Omega}{R_{11}} = 1 + \frac{50\,000\,\Omega}{1\,000\,\Omega} = 51$
Note: *while this initial gain value was selected to protect the preamplifier from saturation caused by low frequency noise at a time when the passive filter in the input section had not yet been implemented, this gain was later found to be slightly on the low side, resulting in the circuit being somewhat insensitive to small input signals* ($< 0.5 - 0.7V$).

1) Current limiting resistor: User-protection resistors R19 and R20 ($2.2\,\text{k}\Omega$) are placed in series with each instrumentation amplifier input. These act as simple current limiters in the event of a catastrophic fault, such as a supply rail or amplifier output accidentally shorting to an input while electrodes are attached to the skin. Assuming a 9 V battery and ignoring skin resistance, the worst-case fault current from a single rail is $I_{\text{fault,single-rail}} \approx \frac{V_{\text{battery}}}{R_{\text{series}}} = \frac{9\,\text{V}}{2.2\,\text{k}\Omega} \approx 4.1\,\text{mA}$ and roughly twice this ($\approx 8.2\,\text{mA}$) if, in some way, both rails were simultaneously shorted through the patient path. This is far below typical "macro"-shock danger levels, but still several orders of magnitude higher than the microampere-level patient leakage limits specified for type b/bf applied parts in IEC 60601-1 (100 µA in normal condition and 500 µA in single-fault condition)[7], [8] . The series resistors therefore improve safety compared to an unprotected input stage, but the overall system should be regarded as an educational prototype rather than compliant medical equipment.

2) Bias-network: matched (0.5% tolerance) $1\,\text{M}\Omega$ resistors R9/R18 tie each input to the reference node, providing a DC return path for INA128 bias currents and preventing charge build-up on the input coupling capacitors C4/C10. A $2\,\text{M}\Omega$ resistor R24 between the inputs completes a bias network that sets the DC operating point and improves common-mode behavior [9].. This network shifts the pre-INA high-pass corners slightly above the original 20 Hz target, but the bandwidth still covers the EMG passband while providing stronger attenuation of very low-frequencies. Since our primary goal is robust motor control and not diagnostic-grade EMG, these extra input components (beyond the protection resistors) are mainly included for improved biasing and common mode behavior, educational purposes, and to support potential future use of the circuit for more direct EMG monitoring. Built in the spirit of a professional device.

D. Filtering

Various filtering stages were implemented:

1) **Passive pre-INA high-pass:** a first-order RC high-pass filter is placed *before* the instrumentation amplifier to reduce low-frequency, high-energy motion artifacts that could otherwise overload a high-gain frontend. With $C4/C10 = 7.5\,\text{nF}$ and the bias network $R_{\text{to ref}} \approx R18 \parallel (R24{+}R9) \approx 750\,\text{k}\Omega$, the common-mode corner frequency is $f_{c,\text{CM}} \approx \frac{1}{2\pi\left(R18\|(R24+R9)\right)\cdot 7.5\,\text{nF}} \approx \frac{1}{2\pi\cdot 0.75\,\text{M}\Omega\cdot 7.5\,\text{nF}} \approx 28.3\,\text{Hz}$ slightly above the intended $f_c \approx 21.2$ Hz based on the initial $1\,\text{M}\Omega$ estimate. For differential signals, the two coupling capacitors appear in series, giving an effective differential capacitance $C_{\text{diff}} = 3.75\,\text{nF}$, while the resistor network reduces to $R_{\text{diff}} = R24 \parallel (R18{+}R9) = 1\,\text{M}\Omega$. The differential cutoff becomes: $f_{c,\text{DIFF}} \approx \frac{1}{2\pi R_{\text{diff}} C_{\text{diff}}} \approx \frac{1}{2\pi\cdot 1\,\text{M}\Omega\cdot 3.75\,\text{nF}} \approx 42\,\text{Hz}$.
2) **Post INA: second-order high-pass:** two identical first-order high-pass stages ($R = 7.8\,\text{k}\Omega$, $C = 1\,\mu\text{F}$, $f_c \approx 20.4\,\text{Hz}$) are cascaded, each followed by a TL072 voltage follower to avoid loading. The result is a second-order high-pass filter with a slope of approximately $40\,\text{dB/dec}$. Because both stages share the same cutoff frequency, the combined response is ≈ -6 dB at 20 Hz, rather than the -3 dB of a Butterworth alignment. However, this is acceptable and provides stronger suppression

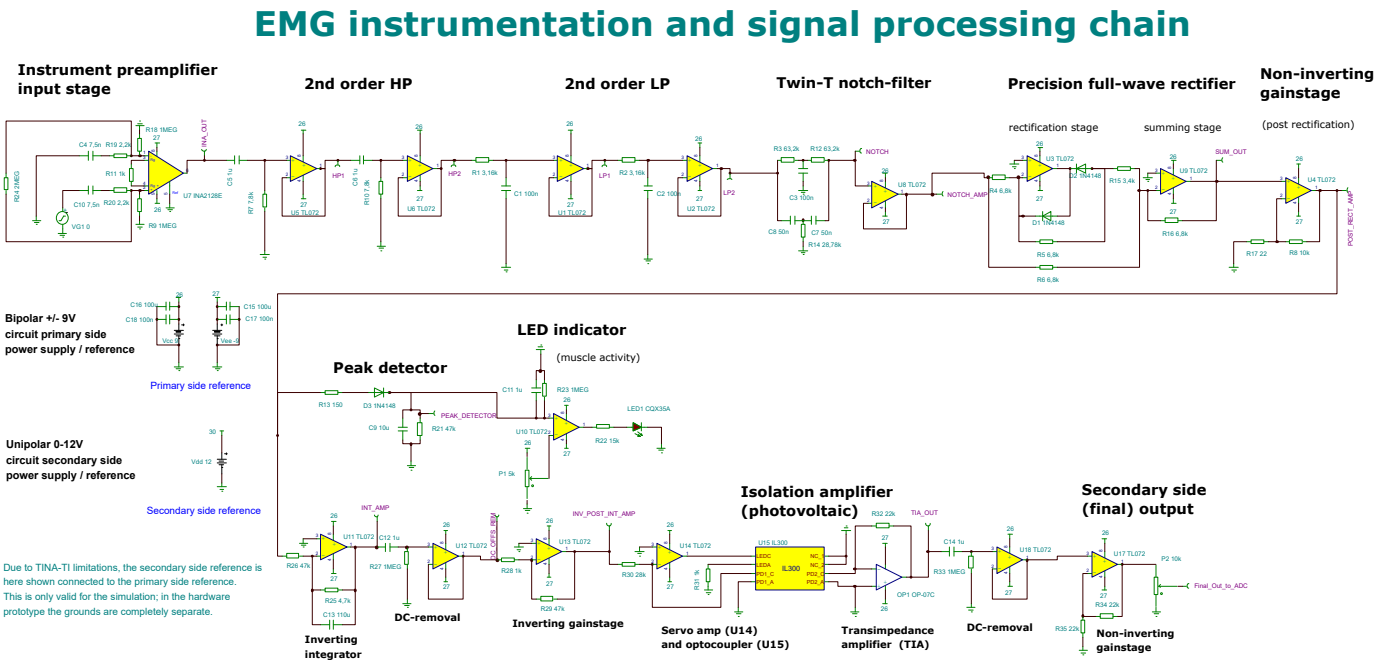

Fig. 2: Complete EMG signal acquisition and processing circuit schematic. If direct EMG monitoring is desirable, it can be taken from the "NOTCH_AMP" output pin. Not shown in the schematic are $0.1\,\mu$F decoupling capacitors placed close to each op-amp (and INA) supply rail pins to 0 V.

of low frequencies and electrode drift while preserving the EMG band above roughly 50 Hz.

3) **Second-order low-pass (LP) at 500 Hz:** a similar structure using two buffered first-order RC stages in cascade provides an overall second-order low-pass response with a slope of 40 dB/dec and a cutoff around 500 Hz.
4) **50 Hz notch (Twin-T):** a passive Twin-T notch is tuned to 50 Hz (local mains frequency) and buffered by a voltage follower. Simulation shows $\approx 30-35$ dB attenuation at the notch frequency, providing substantial rejection of mains interference.

E. Rectification

A precision full-wave rectifier was implemented by combining a precision half-wave rectifier with an inverting summing stage. The first op-amp generates a rectified version of the EMG signal, while the second op-amp sums this with the original input. In the summing stage, the rectified path is given twice the gain of the direct path. During negative half-cycles, this extra factor both cancels the negative contribution of the original signal and recreates a positive copy of the same magnitude, so the final output has appx. the same gain for positive and negative halves of the EMG waveform[10].

F. Non-inverting amplification

A non-inverting amplifier stage was introduced after the rectification block during early testing with a peak-detection-based control scheme. The intention was to maintain phase consistency when the non-inverting "Peak Hold" circuit was utilized. When the design later transitioned to the integrator approach, this stage was retained. This stage provides the majority of the system's voltage gain: $A_v = 1 + \frac{R_f}{R_g} = 1 + \frac{10\,\text{k}\Omega}{22\,\Omega} \approx 454.5$.

In hindsight, this results from an under-sized gain choice in the instrumentation amplifier stage. Distributing gain earlier in the signal chain is generally preferred to improve the signal-to-noise ratio and reduce the possibility of noise amplification at later stages. However, for the specific application here—providing a control signal to a robotic actuator—this gain distribution does not introduce instability or functional issues; therefore, the stage remains in use.

G. Integrating amplifier

The design initially used a "Peak Hold" circuit under the assumption that a rapid response to muscle activation would be desirable. In practice, this type of processing is more suitable for visual clipping indication (the original circuit was adapted from an LED peak indicator in a VU-meter driver circuit). The stage was therefore replaced by an inverting integrator, which converts the rectified EMG bursts into a smooth envelope with moderated rise *and* fall times (as opposed to only the fall time in the peak circuit), yielding a more continuous and proportional control signal for servo motion. The integrating capacitance is implemented using two $220\,\mu$F electrolytic capacitors in series, negative-to-negative, forming an effective non-polarized capacitance of appx. $110\,\mu$F. This value was selected empirically to obtain a response time that felt natural during control tests. The envelope time constant is set by the feedback network $R_{25} \parallel C_{13}$, which behaves as a first-order system with $\tau = R_{25}C_{13} = 4.7\,\text{k}\Omega \cdot 110\,\mu\text{F} \approx 0.52\,\text{s}$, corresponding to a corner frequency $f_c = \frac{1}{2\pi R_{25} C_{13}} \approx 0.31\,\text{Hz}$. This single time constant governs both the rise and fall behavior of the integrated EMG envelope.

H. LED indication

A simple LED indicator with an adjustable threshold was retained to provide visual feedback of muscle activity while tuning the gain distribution in the circuit.

I. Inverting amplification stage

The integrator stage is inherently inverting, resulting in a phase inversion relative to the original EMG signal envelope. To restore the expected polarity, an inverting amplifier stage was added following the integrator. Some adjustable gain was included: $|A_v| = 47$. This allows control over the final signal level feeding the isolation amplifier and, thus, the IR-LED on the optocoupler's primary side.

J. Isolation amplifier, LED driver and TIA

A Vishay IL300 optocoupler provides isolation between the battery-powered sensor circuitry and the Arduino/Braccio control side. Isolation is achieved through optical transmission across a non-conductive barrier, keeping both sides electrically separate with their own supplies and references [11]. The IL300 requires a servo amplifier (U14) to drive the LED on the primary side and a transimpedance amplifier (OP07) on the secondary side to convert the photodiode current into a voltage for the Arduino ADC. The circuit follows the photovoltaic configuration from the application notes, using $28\,\mathrm{k}\Omega$ on the primary side and a $22\,\mathrm{k}\Omega$ TIA resistor on the secondary side, giving an approximate gain of $A_v \approx \frac{K_2}{K_1} \cdot \frac{R_{\text{secondary}}}{R_{\text{primary}}} \approx 1 \cdot \frac{22\,\mathrm{k}\Omega}{28\,\mathrm{k}\Omega} \approx 0.79$.

K. Final Non-Inverting Amplification and DC Offset Removal

To remove the residual DC offset from the TIA stage, a $1\,\mu$F coupling capacitor and R_{33} form a high-pass filter that blocks DC while passing the EMG envelope. The AC-coupled signal is then buffered and amplified by a final non-inverting stage with adjustable gain, providing level control before digitization and preserving signal polarity.

L. Powersupply

Bipolar ± 9 V batteries powered the sensor front end, while the post-optocoupler circuitry operated from a unipolar supply. The original intention was to run the secondary-side op-amps from the Arduino's 0–5 V rail for inherent ADC protection, but the TL072 is not specified for such low supply voltages (recommended $V_{\text{S,min}} = 10$ V and an input range of roughly $V_{\text{CC-}} + 4$ V to $V_{\text{CC+}} - 4$ V)[12]. The secondary side was therefore powered from an external 12 V source; in a refined design, rail-to-rail low-voltage op-amps would be preferred.

Both supply rails and reference grounds remain isolated across the optocoupler, preserving full galvanic isolation between the body-connected front end and the Arduino acquisition side. This completes the analog EMG signal path.

III. Photoplethysmography Sensor System

A. PPG Operating Principles

Photoplethysmography exploits the optical properties of biological tissue to measure cardiovascular activity non-invasively. The technique employs light-emitting diodes (LEDs) to illuminate tissue, while photo-diodes detect the transmitted (or reflected) light intensity. Hemoglobin's strong wavelength-dependent absorption causes the detected light to modulate with changes in arterial blood volume during each cardiac cycle [13].

The PPG signal comprises two primary components. The AC component, representing pulsatile arterial blood flow, oscillates at the heart rate frequency (typically 0.5–5 Hz, corresponding to 30–300 beats per minute). The DC component, which reflects the semi-static optical properties of tissue, including skin, fat, bone, and venous blood, changes slowly with respiration (< 0.5 Hz)[3]. Caizonne et al. [14] writes, "The AC component is only a fraction (typically below 10%) of the DC component, depending on the body location and skin tone". This results in the AC-component superimposed upon the much larger DC-baseline.

B. Wavelength Selection and Optical Configuration

Typical PPG components use green (495–570 nm), red (655–670 nm) or near-infrared LEDs (880–940 nm) with silicon photodiodes, which exhibit responsivities on the order of 0.3–0.4 A/W at 660 nm and 0.5–0.6 A/W at 940 nm [3].

In this implementation, focusing solely on heart-rate detection, a single WL-TIRC 850 nm infrared LED is paired with an SFH 213 FA photodiode in a transmission configuration on a finger clip: the LED illuminates the fingertip, and the photodiode on the opposite side measures the systolic modulation of the transmitted light [15]. Near-infrared light was chosen instead of green to allow use across a wider range of skin tones, since green light is more strongly absorbed by melanin and may not reach the vascular tissue in users with darker skin [16].

C. Transimpedance Amplifier

Photodiodes function as light-driven current sources, generating photocurrents that are roughly proportional to the incident optical power. Converting these currents to voltages is achieved using a transimpedance amplifier (TIA). In our design, a TL072CP op-amp is configured as a TIA with a $1\,\mathrm{M}\Omega$ feedback resistor R_f from the output to the inverting input, and the photodiode (SFH 213 FA) is connected between the inverting node and ground. The non-inverting input is biased slightly above ground by a resistive divider so that, for zero or low photocurrent, the output rests within the linear region of the op amp rather than at a supply rail. This follows standard single-supply photodiode amplifier practice, where a reference voltage V_{ref} on the non-inverting input prevents saturation at the negative rail[17].

With this configuration, the output voltage can be expressed as $V_{\text{out}} \approx V_{\text{ref}} - I_{\text{PD}} \cdot R_f$

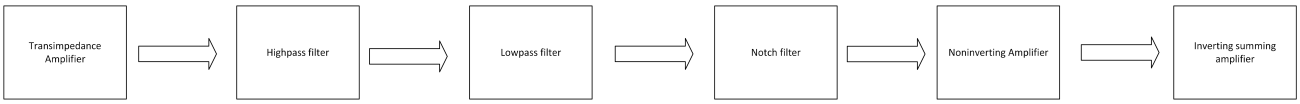

Fig. 3: PPG signal pathway

D. Filters

The high-pass and low-pass filters together form a band-pass filter with a 0.5–5 Hz passband, chosen to capture heart rates of roughly 60–180 bpm (1–3 Hz) with some margin. The notch filter is centered at 50 Hz to attenuate mains interference. The high-pass uses a $470\,\mathrm{k}\Omega$ resistor and a $0.68\,\mu$F capacitor, while the low-pass uses $150\,\mathrm{k}\Omega$ and $0.22\,\mu$F. The notch filter is implemented as a twin-T network with component values $33k\Omega$, $68k\Omega$, $47nF$ and $100nF$. The filters are buffered using TL072CP in a voltage follower configuration to avoid interference between the respective RC-networks.

PPG measurements are affected by motion artifacts and ambient lighting, which occur in the 0.1-20 Hz range [16]. This noise overlaps with the frequency of the PPG signal, which can make it challenging to eliminate noise from the signal.

E. Non-inverting Amplifier

After filtering, the signal is buffered and fed to a non-inverting stage with gain: $A_v = 1 + \frac{R_f}{R_1} = 1 + \frac{47\,\mathrm{k}\Omega}{3.9\,\mathrm{k}\Omega} \approx 13$ A non-inverting configuration was chosen so that the PPG signal is only inverted in the final stage; since the photodiode senses transmitted (unabsorbed) light, inverting it at the end produces an output that visually resembles a positive-going pulse waveform.

F. Voltage Divider

A resistive voltage divider is used to generate an offset voltage that is summed with the PPG signal so that the entire waveform is shifted from $\pm 9V$ to the unipolar 0–5 V input range of the microcontroller ADC.

G. Inverting Summing Amplifier

The final PPG stage is an inverting summing amplifier that combines the amplified PPG signal with the DC offset from the divider. It uses a TL072CP with a $10\,\mathrm{k}\Omega$ feedback resistor from output to the inverting input. The output is given by $V_{\text{out}} = -\frac{R_f}{R_{\text{in}}} V_{\text{PPG}} - \frac{R_f}{R_{\text{DC}}} V_{\text{offset}}$, where R_{in} and R_{DC} are the input resistors for the PPG path and the DC reference. This stage both inverts the waveform (producing a positive-going pulse) and shifts it into the ADC's usable range.

IV. Acquisition & Control

A. Arduino ADC Characteristics

The Arduino micro-controller incorporates a successive-approximation 10-bit analog-to-digital converter with a 5 V reference voltage by default. This provides a quantization resolution of: $\Delta V = \frac{5\,\mathrm{V}}{2^{10}} = \frac{5\,\mathrm{V}}{1024} \approx 4.88\,\mathrm{mV}$ The ADC produces integer output codes from 0 to 1023, corresponding to input voltages from 0 to 5 V according to: $\mathrm{Code} = \left\lfloor \frac{V_{\text{in}}}{V_{\text{ref}}} \cdot 1024 \right\rfloor$

B. Threshold-Based Control Algorithm

The robotic arm control-system code employs a simple threshold detection scheme. When the digitized bio-signal crosses a predetermined voltage level, the micro-controller issues motion commands to the Braccio robotic arm. this is achieved through a PWM (Pulse-Width Modulation) signal, where the length of the high-time of the signal indicates the direction and final angle for the servo movement. The implemented firmware instead uses two explicit thresholds defined in ADC counts: THRESHOLD1=**50** (≈0.24\approx 0.24≈0.24 V) THRESHOLD2=**720** (≈3.5\approx 3.5≈3.5 V)

V. Results

A. EMG circuit

1) Measurement Procedure: The frequency response of the EMG front-end was measured by manually sweeping the input frequency and recording the corresponding input amplitude (at the electrode connection node) and output amplitude and phase (at the buffered notch-filter output, before rectification). Some variation in the measured input (and corresponding output) levels was observed, possibly due to the interaction between the generator's $50\ \Omega$ source impedance and the frequency-dependent input impedance of the circuit. Two measurement cycles with a sine wave at 200 $\mathrm{mV_{pp}}$ and 2 $\mathrm{V_{pp}}$, respectively, were applied to the INA128 non-inverting input, with the inverting input tied either to ground or to an identical sine wave of opposite polarity for differential excitation. Calculating $20\log_{10}\left(\frac{V_{\text{out}}}{V_{\text{in}}}\right)$ at each test frequency, the discrete transfer magnitude was yielded, and plotting these points produced the measured frequency response of the circuit. This was then compared with the TINA-TI simulation results.

TABLE I: Key EMG Circuit Performance Metrics

Metric	200mVpp	2Vpp	Simulation	Spec
Peak Gain (dB)	25.4	28.3	29.7	∼ 25 - 30
Peak Freq (Hz)	300	200	263	∼ passband
50 Hz Depth (dB)	-3.6	1.1	-2.8	∼ 0
Notch Rej.[a] (dB)	29.0	27.3	32.5	>25
Passband BW (Hz)	∼ 350	∼ 400	393	300–500
Gain at Key Frequencies (dB):				
2 Hz	-11.0	-27.5	-25.8	—
20 Hz	12.0	13.4	18.0	—
500 Hz	23.4	25.7	27.1	—
5 kHz	-5.2	-12.6	-5.1	—
HP Rolloff (dB/dec)	∼ 23	∼ 41	∼ 44	40-60
LP Rolloff (dB/dec)	∼ 29	∼ 38	∼ 32	40

[a]Rejection calculated relative to peak passband gain.

2) Results summary: Frequency response shows the expected high-pass transition, 50 Hz notch shift, and low-pass roll-off. Figure 4 shows agreement between simulation and measurements across the chosen EMG band, while Figure 5 provides detailed views of critical filter regions.

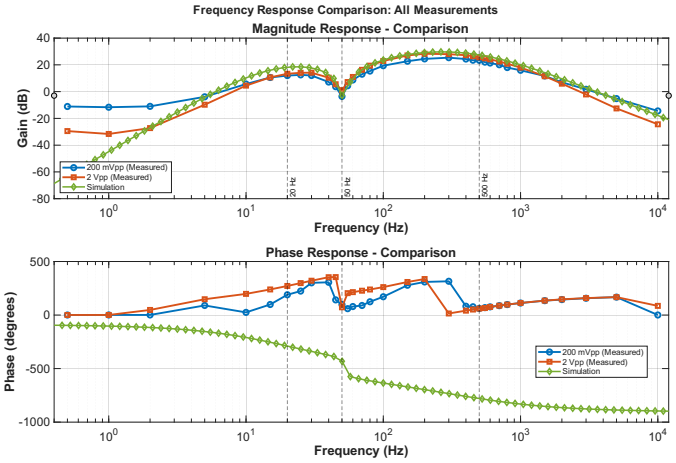

Fig. 4: Comparison of simulation (green) with hardware measurements at 200 mVpp (blue) and 2 Vpp (red).

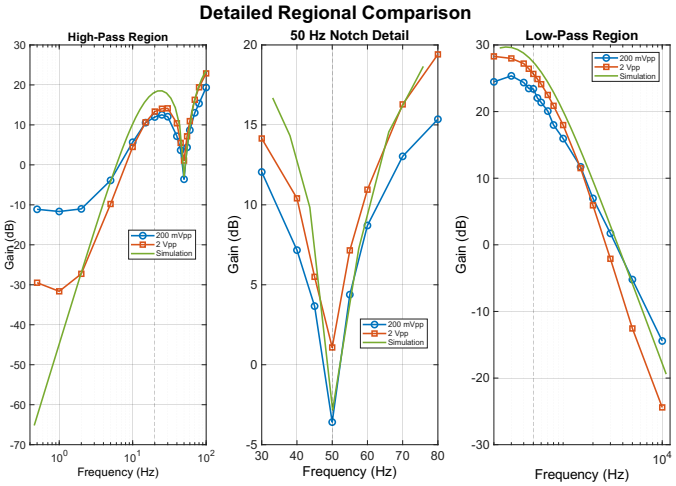

Fig. 5: Detailed view of high-pass, notch, and low-pass transition regions.

The EMG front-end delivers stable gain, strong 50 Hz suppression, and adequate bandwidth for EMG acquisition within the 20–500 Hz range. Measured and simulated magnitude responses agree within 1–6 dB across the EMG band. The "raw" EMG signal is shown in Fig. 6a, while the final processed signal fed to the Arduino is shown in Fig. 6b.

B. PPG circuit filters

Using a Tektronix AFG1022 signal generator to test the frequency response of the LP–HP–Notch filter circuit yielded the following results. At a signal frequency of 0.5 Hz, the attenuation was (Fig. 8): $A_{0.5\text{Hz}} = 20\log_{10}\left(\frac{1.1440}{2.080}\right) = -3.19$ dB. This shows that the low-pass filter response is close to the intended cutoff frequency.

At 5 Hz, the attenuation was $A_{5\text{Hz}} = 20\log_{10}\left(\frac{1.340}{2.120}\right) = -3.98$ dB. The slightly higher-than-expected attenuation may be due to oscilloscope noise, since it registered the generator output as 2.120 V instead of 2 V (Fig. 9).

At 50 Hz, the attenuation was $A_{50\text{Hz}} = 20\log_{10}\left(\frac{0.08}{2.080}\right) = -28.29$ dB, demonstrating strong suppression of mains interference (Fig. 10).

The strong attenuation at 50 Hz demonstrates that the notch filter, in combination with the low-pass stage, effectively suppresses mains interference (Fig. 10).

C. PPG circuit output signal

The PPG circuit produces a clean pulse-shaped output due to the final inverting stage. The incoming signal represents transmitted IR light; during systole, the TIA output voltage decreases. Inversion produces a rising waveform corresponding to systolic peaks. Because the DC offset from the voltage divider is summed with the PPG signal in the final stage, the entire waveform remains within the 0–5 V ADC range, ensuring full capture of the pulse waveform (Fig. 11).

VI. Conclusions

This project successfully demonstrated the integration of biomedical sensor technologies with robotic control systems through a comprehensive analog and digital signal processing chain. The EMG sensor system achieved the necessary amplification and noise reduction to detect muscle activity signals, while the PPG sensor system reliably extracted cardiovascular information from optical measurements, despite the challenging AC-on-DC signal characteristics.

Future enhancements could incorporate multi-channel EMG sensing for proportional control and gesture recognition, dual-wavelength PPG implementation enabling pulse oximetry functionality, and more sophisticated digital signal processing techniques, such as adaptive filtering for improved noise cancelation.

References

[1] W. M. B. Wan Daud et al., "Features extraction of electromyography signals in time domain on biceps brachii muscle," *International Journal of Modeling and Optimization*, vol. 3, pp. 515–519, Dec. 2013.

[2] R. Ismail, "Muscle power signal acquisition monitoring using surface EMG," *Journal of Biomedical Research & Environmental Sciences*, vol. 3, no. 5, pp. 663–667, May 2022.

[3] E. Mejía-Mejía et al., "Photoplethysmography signal processing and synthesis," in *Photoplethysmography*, Elsevier, 2022, pp. 69–146.

[4] E.-G. Han et al., "Physiological signal-based real-time emotion recognition based on exploiting mutual information with physiologically common features," *Electronics*, vol. 12, p. 2933, Jul. 3, 2023.

[5] P. Liu et al., "Medical intelligence using PPG signals and hybrid learning at the edge to detect fatigue in physical activities," *Scientific Reports*, vol. 14, no. 1, p. 16 149, Jul. 12, 2024.

[6] M. Al-Ayyad et al., "Electromyography monitoring systems in rehabilitation: A review of clinical applications, wearable devices and signal acquisition methodologies," *Electronics*, vol. 12, no. 7, p. 1520, Jan. 2023.

[7] *Medical electrical equipment — part 1: General requirements for basic safety and essential performance*, International Standard, Geneva, Switzerland: International Electrotechnical Commission, Aug. 2012.

[8] A. Energy. “Safety requirements in medical equipment: Designing for bf and cf classifications.”
[9] Texas Instruments, *INA12x Precision, Low-Power Instrumentation Amplifiers datasheet (Rev. F)*. Nov. 8, 2025.
[10] D. Das. “Half wave and full wave precision rectifier circuit using op-amp,” Circuit Digest.
[11] D. Görk et al., “Designing linear amplifiers using the il300 optocoupler,” Vishay Semiconductors, Application Note 83708 (Application Note 50), Oct. 2021.
[12] T. Instruments, “Tl07xx low-noise, fet-input operational amplifiers data sheet (tl071, tl072, tl074),” Texas Instruments, Data Sheet SLOS080W, 2025.
[13] M. Nichol et al., “Pulse oximetry: Fundamentals and technology,” *Respiratory Care*, 2013.
[14] A. Caizzone et al., “AC/DC ratio enhancement in photoplethysmography using a pinned photodiode,” *IEEE Electron Device Letters*, vol. 40, no. 11, pp. 1828–1831, Nov. 2019.
[15] H. L. Lujan et al., ““seeing red” reflects hemoglobin’s saturation state: A discovery-based activity for understanding the science of pulse oximetry,” *Advances in Physiology Education*, vol. 46, no. 3, pp. 461–467, Sep. 2022.
[16] J. Fine et al., “Sources of inaccuracy in photoplethysmography for continuous cardiovascular monitoring,” *Biosensors*, vol. 11, no. 4, p. 126, Apr. 2021.
[17] Texas Instruments, “Photodiode amplifier circuit,” Texas Instruments, Tech. Rep. SBOA220B, 2018.

APPENDIX

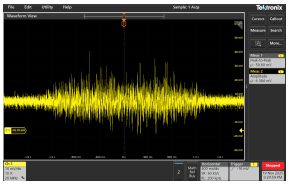

(a) “Raw” EMG from `NOTCH_OUT`. INA128 gain 51 gives $60\,\mathrm{mV} \approx 1.17\,\mathrm{mV}$ biological.

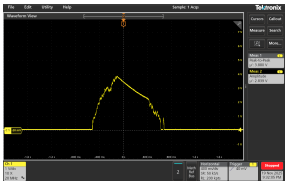

(b) Final rectified and integrated EMG control signal.

Fig. 6: Raw EMG waveform vs. final control envelope.

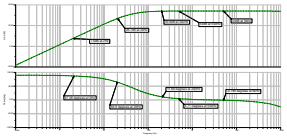

(a) Preamp and input section Bode plot.

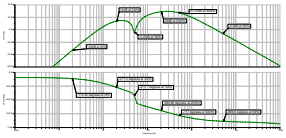

(b) Overall accumulated frequency response.

Fig. 7: Simulated EMG front-end responses.

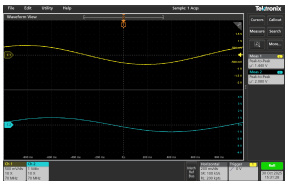

Fig. 8: PPG filter test at 0.5 Hz, $2\,\mathrm{V_{pp}}$.

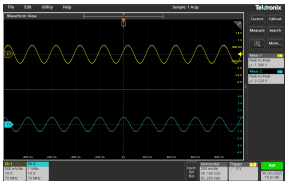

Fig. 9: PPG filter test at 5 Hz, $2\,\mathrm{V_{pp}}$.

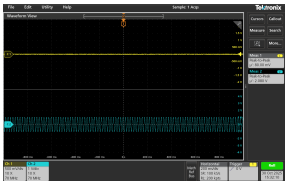

Fig. 10: PPG filter test at 50 Hz, $2\,\mathrm{V_{pp}}$.

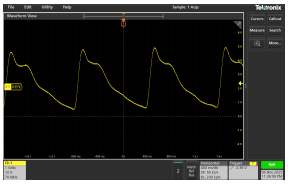

Fig. 11: PPG output signal with finger inserted.